Defence Technology 18 (2022) 205–218

Contents lists available at ScienceDirect

Defence Technology

journal homepage: www.keaipublishing.com/en/journals/defence-technology

Buckling analysis of shear deformable composite conical shells reinforced by CNTs subjected to combined loading on the two-parameter elastic foundation

A.H. Sofiyev [a, b, c, *], N. Kuruoglu [d]

[a] Department of Civil Engineering of Engineering Faculty, Suleyman Demirel University, 32260, Isparta, Turkey
[b] Information Technology Research and Application Center Member of Consultancy Board of ITRAC Center, Istanbul Commerce University, Beyoglu, 34445, Istanbul, Turkey
[c] Scientific Research Centers for Composition Materials of UNEC-Azerbaijan State Economic University, 1001/Baku, Azerbaijan
[d] Department of Civil Engineering of Faculty of Engineering and Architecture of Istanbul Gelisim University, Istanbul, Turkey

ARTICLE INFO

Article history:
Received 5 November 2020
Received in revised form
4 December 2020
Accepted 30 December 2020
Available online 20 January 2021

Keywords:
Nanocomposites
CNTs
Composite conical shells
Two-parameter elastic foundations
Combined buckling loads
Shear deformation shell theories

ABSTRACT

The main objective of this study is to investigate the buckling analysis of CCSs reinforced by CNTs subjected to combined loading of hydrostatic pressure and axial compression resting on the two-parameter elastic foundation (T-P-EF). It is one of the first attempts to derive the governing equations of the CCSs reinforced with CNTs, based on a generalized first-order shear deformation shell theory (FSDST) which includes shell-foundation interaction. By adopting the extended mixing rule, the effective material properties of CCSs reinforced by CNTs with linear distributions are approximated by introducing some efficiency parameters. Three carbon nanotube distribution in the matrix, i.e. uniform distribution (U) and V and X-types linear distribution are taken into account. The stability equations are solved by using the Galerkin procedure to determine the combined buckling loads (CBLs) of the structure selected here. The numerical illustrations cover CBLs characteristics of CCSs reinforced by CNTs in the presence of the T-P-EF. Finally, a parametric study is carried out to study the influences of the foundation parameters, the volume fraction of carbon nanotubes and the types of reinforcement on the CBLs.

1. Introduction

The importance of shell theories in modern science and technology is growing every day. While the theory of plates and shells solves the rational tasks of designing engineering structures, which consisted mainly of finished materials, at the present time, the optimal design and production of the materials that make up the structures play a more active role. Recently, using new technological methods, developing the properties of the various materials that make up the structural elements, designs are created with high performance and low cost [1,2].

Due to its high aspect ratio, large surface area, rich surface chemical functionality and nanoscale dimensional stability, CNTs have various applications such as electromagnetic interference protection, membranes and structural reinforcement. CNTs have the simplest chemical composition and atomic bonding configuration, adding extraordinary variety and richness in the properties of the structures. The CNTs were discovered by Sumio Iijima in 1991, shortly after the laboratory synthesis of fuller in the installation of the arc discharge apparatus [3].

In modern technology, there is a need for lightweight, flexible and durable alternatives to replace hard and brittle materials. Instead of traditional materials that have been used for thousands of years, synthetic materials today can be produced at the scale of atoms, including CNTs. The nanotubes are a structural element made by bending graphene, which consists of one row of carbon atoms, into a cylinder. Even though it has such a simple shape, it becomes more effective as its physical and chemical properties change as the length and diameter change. The carbon nanotubes, which can reach a diameter of millions of times, are more beneficial

* Corresponding author. Department of Civil Engineering, Suleyman Demirel University, 32260, Isparta, Turkey.
E-mail addresses: abdullahavey@sdu.edu.tr (A.H. Sofiyev), nkuruoglu@gelisim.edu.tr (N. Kuruoglu).
Peer review under responsibility of China Ordnance Society

https://doi.org/10.1016/j.dt.2020.12.007

than other materials due to their properties such as strength, electrical conductivity, and thermal conductivity [4,5].

The superior properties of CNTs open up exciting possibilities for new composites. NASA has invested heavily in the development of carbon nanotube-based composites for applications such as a mission to Mars. Recently, polymer/CNT composites have received great attention due to their unique mechanical, surface and multifunctional properties, as well as their strong interaction with the matrix due to their nanoscale microstructure and extremely large interfaces [6]. Determination of thermal, electrical and mechanical properties of composites reinforced with carbon nanotubes reveals the extraordinary advantages of nanocomposites. Velasco-Santos et al. [7] investigated the effect of multi-walled carbon nanotubes (MWCNTs) and processing methods on the morphological, dynamic, mechanical, mechanical, thermal and electrical properties of MWCNT/nylon 6 (PA6) composites. Moniruzzaman and Winey [8] summarized various nanotube/polymer composite manufacturing methods, including solution mixing, melt mixing, and in-situ polymerization, with special emphasis on evaluating the dispersion state of nanotubes. In addition, mechanical, electrical, rheological, thermal, and flammability are specifically discussed, and the variation of these physical properties depending on the size, aspect ratio, loading, distribution status and alignment of nanotubes in polymer nanocomposites is discussed. Alizada and Sofiyev [9] created modified Young's moduli of nanomaterials taking into account the scale effects and vacancies. Díez-Pascual et al. [10] presented research on the production of single-walled carbon nanotube buckypaper reinforced poly (phenylene sulphide) and poly (ether-ether ketone) composite laminates by hot press process using transmission electron microscopes.

The advent and widespread use of carbon nanotubes led to the development of new generation heterogeneous composite structures based on polymers. The defense industry is undoubtedly one of the earliest manufacturers of advanced composites, in particular CNT-reinforced composites. This is due to the fact that the defense industry requires materials with low weight, high strength and stiffness. The composite circular shells reinforced by CNTs, combining lightness with high strength are widely used in many branches of the modern defense industry, such as submarines, aircraft and spaceships, rockets, pressure vessels, for military drones, armored military vehicles, etc., and are subjected to various combined loads. It is of great technical importance to clarify the buckling behavior of heterogeneous composite shells under combined loadings. Although not many, there are some remarkable studies on this problem. The buckling problem of heterogenous composite cylindrical shells reinforced with carbon nanotubes under combined loads was first mathematically modeled and solved in the study of Shen and Xiang [11]. After this study, the stability problems of rotating cylindrical shells reinforced by CNTs and nano-shells under combined loadings were solved in various formulations [12,13]. Later Sofiyev et al. [14] presented a solution to the problem of stability of composite conical shells reinforced with carbon nanotubes under combined loads.

Due to structural elements reinforced by CNTs are used in a variety of environments, the influence of elastic media on their behavior is crucial for safety. One of the more frequently used models that better define the structure of elastic foundations is the two-parameter elastic foundation model or Pasternak model [15]. The special case of the Pasternak model is the one-parameter elastic foundation model or Winkler elastic foundation model (W-EF), which is defined as a system of parallel springs that do not touch each other [16]. In addition to these models, basic information about other foundation models and their interactions with structural members are also presented in Ref. [17]. The interaction of the homogeneous conical shells with the two-parameter elastic foundation (T-P-EF) and the solution of bending problems suggested by Sun and Huang [18].

The use of advanced composites in unmanned aerial vehicles, armor of tanks and aircraft, wing and empennage elements of aircraft and runways, especially on ships, submarines and oil transportation, makes a significant contribution to the development of various industries, including the defense industry. Since 2014, research has been conducted on the stability and vibrational characteristics of structural elements reinforced with CNTs resting on the EFs. For example, the influence of the two-parameter elastic foundation on the buckling or vibration behaviors of the composite plates and panels reinforced with carbon nanotubes has been studied in various formulations and theories. Zhang et al. [19] studied vibration for functionally graded carbon nanotube-reinforced composite thick plates resting on elastic foundations using the element-free IMLS-Ritz method. Fu et al. [20] analyzed the nonlinear dynamic stability of carbon nanotube-reinforced composite plates resting on elastic foundations. Bani'c et al. [21] examined influence of Winkler-Pasternak foundation on the vibrational behavior of plates and shells reinforced by agglomerated carbon nanotubes. Tounsi and coauthors [22–25] investigated the buckling and vibration behaviors of FGM and FG-CNT mono and sandwich plates made of new generation materials on the elastic foundations using different boundary conditions and theories. Shen and Xiang [26–29] investigated nonlinear vibration and post-buckling of nanotube-reinforced composite cylindrical panels under axial and external pressures resting on elastic foundations in thermal environments. Mohammadi et al. [30] studied higher-order thermo-elastic analysis of FG-CNTRC cylindrical vessels surrounded by a Pasternak foundation. Duc et al. [31] presented thermal and mechanical stability of functionally graded carbon nanotubes (FG CNT)-reinforced composite truncated conical shells surrounded by the elastic foundations.

It is known that the influences of shear strains are very important for the buckling behavior of composite shells in different environments. The use of shear deformation shell theories (SDSTs) in the calculation of the critical parameters of composite shells allows one to overcome the disadvantages of the critical parameters when using CST [31–35]. In recent years, various methods have been developed for studying the problems of stability and vibration of heterogeneous composite shells in different environments based on the SDSTs. Bousahla et al. [36] studied buckling and dynamic behavior of the simply supported CNT-RC beams using an integral-first shear deformation theory. Babaei et al. [37] reported thermal buckling and post-buckling analysis of geometrically imperfect FGM clamped tubes on nonlinear elastic foundation. Sobhy and Zenkour [38,39] studied vibration and hygrothermal analysis of functionally graded graphene platelet-reinforced composite doubly-curved shallow shells and microplates on elastic foundations.

As can be seen from the literature review, no scientific studies have been carried out regarding the problem of loss of stability of CCSs reinforced with CNTs under combined loads, taking into account the influence of T-P-EF in the framework of the FSDST. The main purpose of this study is to examine the solution of this problem in detail. The study consists of the following sections: the first section is an introduction that evaluates the literature studies relevant to this study and presents the original features of the article. In sections 2 and 3, taking into account the T-P-EF effect, the problem is formulated and the basic equations are derived. In section 4, the basic differential equations are solved for specific boundary conditions, and a new and original expression for the combined buckling loads is obtained. After proving the correctness of the formulas obtained by comparison in Section 5, an original

$$E_{11\bar{z}} = \eta_1 V_{CN} E_{11}^{CN} + V^m E^m,\ \frac{\eta_2}{E_{22\bar{z}}} = \frac{V^{CN}}{E_{22}^{CN}} + \frac{V^m}{E^m},\ \frac{\eta_3}{G_{12}} = \frac{V^{CN}}{G_{12}^{CN}} + \frac{V^m}{G^m}$$

$$G_{13\bar{z}} = G_{12\bar{z}},\ G_{23\bar{z}} = 1.2\, G_{12\bar{z}},\ \nu_{12} = V_*^{CN}\nu_{12}^{CN} + V^m\nu^m,\ \rho_{\bar{z}} = V^{CN}\rho^{CN} + V^m\rho^m \tag{3}$$

numerical analysis was carried out in the presence of elastic foundations and, finally, the comments are discussed in Section 6.

2. Formulation of the problem

2.1. Geometry and material properties

Consider composite conical shell reinforced by CNTs and resting on the two-parameter elastic foundation under a combined loading (Fig. 1). The symbols characterizing the CCS are presented below: The thickness is h, the large and small radii are a and b, the length of the truncated cone is L, the semi-vertex angle is γ, the distance from the top of the cone to the small and large bases are s_1 and s_2. The origin of the coordinate system is at the top of the cone and located on the middle surface, the x axis is directed along the generator, the θ axis is in the circumferential direction, and the z axis is perpendicular to the plane of these two axes and directed inward. The displacement components of any point on the reference surface in the x, y and $z$directions are shown as u, v and w, respectively. The two-parameter elastic foundation is used as the elastic foundation model and its mathematical expression is as follows [18]:

$$N_0 = k_1 w - \frac{k_2}{s_2^2 e^{2x}}\left(\frac{\partial^2 w}{\partial x^2} + \frac{\partial^2 w}{\partial \theta_1^2}\right) \tag{1}$$

where $\theta_1 = \theta \sin\gamma$, $x = \ln(s/s_2)$, k_1 denotes the stiffness of the spring layer (in Pa/m), k_2 denotes the shearing layer stiffness of the foundation (Pa·m), N_0 is the reaction force of the T-P-EF per unit area on the shell reinforced by CNTs, and a coma is indicated partial differentiation versus the coordinates.

The composite conical shells reinforced by CNTs are subjected to a combined axial load and uniform hydrostatic pressure, as follows [14]:

$$T_x^0 = -T_{ax} - \frac{1}{2}\frac{xP}{\cot\gamma},\ T_\theta^0 = -\frac{xP}{\cot\gamma},\ T_{x\theta}^0 = 0 \tag{2}$$

where T_x^0, T_θ^0, $T_{x\theta}^0$ are the membrane forces for null initial moments, T_{ax} is the axial load, andP_H stands for the uniform hydrostatic pressure.

For convenience and simplicity, the extended mixing rule is used to express the effective material properties of CCSs reinforced by CNTs as follows [11,23]:

where the Young's modulus and shear modulus, Poisson's ratio and density of matrix and CNTs are denoted E^m, G^m, ρ^m, ν^m and E_i^{CN}, G_{12}^{CN}, ρ^{CN}, $\nu_{12}^{CN}(i = 1,2)$, respectively, the efficiency parameters are η_1, η_2 and η_3. Additionally, the volume fractions of CNTs and matrix satisfies the following relationship: $V^{CN} = 1 - V^m$. Here V_*^{CN} depends on density and mass functions of matrix and CNT and defined as [23,26–29]:

$$V_*^{CN} = \frac{w^{CN}}{w^{CN} + (\rho^{CN}/\rho^m) - (\rho^{CN}/\rho^m)w^{CN}} \tag{4}$$

where w^{CN} denotes the mass fraction of nanotubes.

3. Governing relations and equations

The constitutive equations of CCSs reinforced by CNTs with linear distributions in the framework of the FSDST are built as [14]:

$$\begin{bmatrix}\sigma_{11}\\ \sigma_{22}\\ \sigma_{12}\end{bmatrix} = \begin{bmatrix}\overline{E}_{11\bar{z}} & \overline{E}_{12\bar{z}} & 0\\ \overline{E}_{21\bar{z}} & \overline{E}_{22\bar{z}} & 0\\ 0 & 0 & \overline{E}_{66\bar{z}}\end{bmatrix}\begin{bmatrix}\varepsilon_{11}\\ \varepsilon_{22}\\ \gamma_{12}\end{bmatrix} = \begin{bmatrix}\sigma_{13}\\ \sigma_{23}\end{bmatrix}\begin{bmatrix}\overline{E}_{55\bar{z}} & 0\\ 0 & \overline{E}_{44\bar{z}}\end{bmatrix}\begin{bmatrix}\gamma_{13}\\ \gamma_{23}\end{bmatrix} \tag{5}$$

where $\sigma_{ij}(i = 1,2, j = 1,2,3)$ and ε_{ii}, $\gamma_{ij}(i = 1,2, j = 2,3)$ are the stresses and strains of conical shells reinforced by CNTs, respectively and the material constants $\overline{E}_{ij\bar{z}}$ are given by:

$$\overline{E}_{11\bar{z}} = \frac{E_{11\bar{z}}}{1-\nu_{12}\nu_{21}},\ \overline{E}_{22\bar{z}} = \frac{E_{22\bar{z}}}{1-\nu_{12}\nu_{21}},\ \overline{E}_{12\bar{z}} = \frac{\nu_{21}E_{11\bar{z}}}{1-\nu_{12}\nu_{21}} = \frac{\nu_{12}E_{22\bar{z}}}{1-\nu_{12}\nu_{21}} = \overline{E}_{21\bar{z}},$$

$$\overline{E}_{44\bar{z}} = G_{23\bar{z}},\ \overline{E}_{55\bar{z}} = G_{13\bar{z}},\ \overline{E}_{66\bar{z}} = G_{12\bar{z}} \tag{6}$$

In the framework of the generalized first order shear deformation shell theory [14,32] in association with the modified Donnell shell theory, the governing equations for the CCSs reinforced by CNTs with linear distribution under combined loading and resting on the T-P-EF can be derived and expressed by

$$\begin{aligned}
&L_{11}(\Phi) + L_{12}(w) + L_{13}(\Psi_s) + L_{14}(\Psi_\theta) = 0\\
&L_{21}(\Phi) + L_{22}(w) + L_{23}(\Psi_s) + L_{24}(\Psi_\theta) = 0\\
&L_{31}(\Phi) + L_{32}(w) + L_{33}(\Psi_s) + L_{34}(\Psi_\theta) = 0\\
&L_{41}(\Phi) + L_{42EP}(w) + L_{42TPEF}(w) + L_{43}(\Psi_s) + L_{44}(\Psi_\theta) = 0
\end{aligned} \tag{7}$$

where Ψ_s and Ψ_θ are the rotations of the normal to the mid-surface

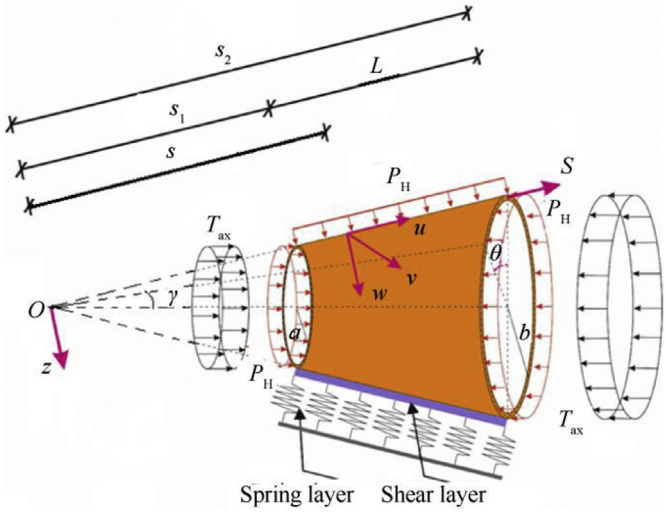

Fig. 1. Composite shell reinforced by CNTs resting on the two-parameter elastic foundation and notations.

with respect to the θ- and s-axes, and Φ is the stress function defined by Refs. [32,40,41].

$$(T_s,\ T_\theta,\ T_{s\theta}) = \frac{h}{s_2^2 e^{2x}}\left(\frac{\partial^2\Phi}{\partial\bar{\theta}^2}+\frac{\partial\Phi}{\partial x},\ \frac{\partial^2\Phi}{\partial x^2}-\frac{\partial\Phi}{\partial x},\ -\frac{\partial^2\Phi}{\partial x\partial\bar{\theta}}+\frac{\partial\Phi}{\partial\bar{\theta}}\right) \tag{8}$$

In the set of Eq. (7), L_{ij} $(i,j=1,2,\ldots,4)$ are differential operators and are defined in Appendix A.

The set of Eq. (7) is the governing equations of carbon nanotube-based heterogeneous CCSs under combined loads and resting on the two-parameter elastic foundation within the FSDST.

4. Solution of governing equations

In this section we present the procedure to solve the eigen value problem, which includes the solution of partially differential equation for freely-supported boundary conditions. The approximation function is sought as follows [14]:

$$\Phi = \overline{\Phi} s_2 e^{(\lambda+1)x}\sin\ (m_1 x)\cos(m_2\bar{\theta}),\quad w = \overline{w}e^{\lambda x}\sin(m_1 x)\cos(m_2\bar{\theta})$$
$$\Psi_s = \overline{\Psi}_s e^{\lambda x}\cos(m_1 x)\cos(m_2\bar{\theta}),\quad \Psi_\theta = \overline{\Psi}_\theta e^{\lambda x}\sin(m_1 x)\sin(m_2\bar{\theta}) \tag{9}$$

where $\overline{\Phi}$, $\overline{w}$, $\overline{\Psi}_s$, $\overline{\Psi}_\theta$ are unknown functions, λ is a parameter that will be determined from the minimum conditions of buckling loads, $m_1 = \frac{m\pi}{s_0}$, $s_0 = \ln\frac{s_2}{s_1}$, $m_2 = \frac{n}{\sin\gamma}$, in which (m, n) are the vibration mode.

Introducing (9) into the system of Eq. (8), then applying the Galerkin procedure to the obtained equations, and using integration and some manipulations, we obtain algebraic equations, which for their non-trivial solution, the determinant of the matrix, consisting of the coefficients of the unknown, equals to zero:

$$\begin{vmatrix} q_{11} & q_{12} & q_{13} & q_{14} \\ q_{21} & q_{22} & q_{23} & q_{24} \\ q_{31} & q_{32} & q_{33} & q_{34} \\ q_{41} & q_{42} & q_{43} & q_{44} \end{vmatrix} = 0 \tag{10}$$

where $q_{ij}(i,j=1,2,\ldots,4)$ are the coefficients depending on the CCSs reinforced by CNTs, $q_{42} = -q_T T_{ax} - q_{PH}P_H - q_{k_1}k_1 - q_{k_2}k_2$ in which q_T and q_{PH} denote coefficients axial compression and hydrostatic pressure, respectively, q_{k_1} and q_{k_2} denote coefficients of the T-P-EF, and are defined in Appendix B.

In order to find the expression for the combined load, we first find the analytical expressions for the axial buckling load and hydrostatic buckling pressure from the extended form of the determinant of Eq. (10).

As the $P_H = 0$, from Eq. (10), we obtain expression for nondimensional axial buckling load (T_{1sdt}^{wpbuc}) for CCSs reinforced by CNTs with linear distributions on the T-P-EF as follows:

$$T_{1sdt}^{wpbuc} = \frac{q_{41}A_1 + q_{43}A_3 + q_{44}A_4}{A_2 E^m h q_T} + \frac{q_{k_1}k_1 + q_{k_2}k_2}{E^m h q_T} \tag{11}$$

where $A_j(j=1,2,3,4)$ are defined as

$$A_1 = -\begin{vmatrix} q_{12} & q_{13} & q_{14} \\ q_{22} & q_{23} & q_{24} \\ q_{32} & q_{33} & q_{34} \end{vmatrix},\ A_2 = \begin{vmatrix} q_{11} & q_{13} & q_{14} \\ q_{21} & q_{23} & q_{24} \\ q_{31} & q_{33} & q_{34} \end{vmatrix},\ A_3 = -\begin{vmatrix} q_{11} & q_{12} & q_{14} \\ q_{21} & q_{22} & q_{24} \\ q_{31} & q_{32} & q_{34} \end{vmatrix},\ A_4 = \begin{vmatrix} q_{11} & q_{12} & q_{13} \\ q_{21} & q_{22} & q_{23} \\ q_{31} & q_{32} & q_{33} \end{vmatrix} \tag{12}$$

As the $P_H = 0$, from Eq. (10), we obtain expression for nondimensional hydrostatic buckling pressure (P_{1sdt}^{wpbuc}) of CCSs reinforced by CNTs with linear distributions on T-P-EF, as follows:

$$P_{1sdt}^{wpbuc} = \frac{q_{41}A_1 + q_{43}A_3 + q_{44}A_4}{A_2 E^m q_{PH}} + \frac{q_{k_1}k_1 + q_{k_2}k_2}{E^m q_{PH}} \tag{13}$$

The critical combined axial load/hydrostatic pressure for CCSs reinforced by CNTs with linear distributions resting on the T-P-EF based on the FSDST, are obtained from the following relation [40]:

$$\frac{T_1}{T_{1sdt}^{wpbuc}} + \frac{P_1}{P_{1sdt}^{wpbuc}} = 1 \tag{14}$$

where $T_1 = T/E^m h$ and. $P_1 = P_H/E^m$

Under the assumptions $T_1 = \mu P_1$, in Eq. (14), we get the following expressions for combined (axial/hydrostatic) buckling load:

$$P_{1sdt}^{wpcb} = \frac{T_{1sdt}^{wpbuc} P_{1sdt}^{wpbuc}}{\mu P_{1sdt}^{wpbuc} + T_{1sdt}^{wpbuc}} \tag{15}$$

Here $\mu \geq 0$ is the dimensionless load-proportional parameter.

By neglecting the shear strains from Eqs. (11), (13) and (15), we

Table 1
The parameters used in numerical analysis and their changes.

Parameters	Changes
Geometrical properties of SWCNT	$\overline{L}=9.26$ nm, $\overline{r}=0.68$ nm $\overline{h}=0.067$ nm
Material properties of SWCNT	$E_{11}^{CN}=5.6466$ TPa, $E_{22}^{CN}=7.0800$ TPa, $G_{12}^{CN}=1.9445$ TPa, $\nu_{12}^{CN}=0.175$, $\rho^{CN}=1400$ kg·m^{-3}
Material properties of PMMA	$E^{m}=2.5$ Pa, $\mu^{m}=0.34$, $\rho^{m}=1150$ kg·m^{-3}
Efficiency parameter of CNT	$\eta_1=0.137$, $\eta_2=1.022$, $\eta_3=0.715$ at $V_{CN}^{*}=0.12$; $\eta_1=0.142$, $\eta_2=1.626$, $\eta_3=1.138$ at $V_{CN}^{*}=0.17$; $\eta_1=0.141$, $\eta_2=1.585$, $\eta_3=1.109$ at $V_{CN}^{*}=0.28$.
Types of profile	UD, VD, XD
One- or two-parameter foundation stiffness	$(k_1,k_2)=(5\times10^8,3\times10^4)$; $(k_1,0)=(5\times10^8,0)$ $(k_1,k_2)=(2.6\times10^9,3.5\times10^4)$
Shear shape functions	$f_i(z)=z-4z^3/3h^2(i=1,2)$
γ	15°, 30°, 45°, 60°
a/h	25, 30, 35, 40

obtain the expressions for the buckling loads T_{1cst}^{wpbuc}, P_{1cst}^{wpbuc} and P_{1cst}^{wpcb}, while neglecting the shear strains. The CBLs for CCSs resting on the one-parameter elastic foundation or Winkler elastic foundation (W-EF) corresponding to $(k_1,0)$. The CBLs for unconstrained shells corresponding to $(k_1, k_2) = (0,0)$will be shown P_{1sdt}^{cb} and P_{1cst}^{cb}.

5. Results and discussion

5.1. Parameters used in numerical calculations

The numerical analyzes are carried out by changing eight parameters: volume fraction of SWCNT, CNT distribution, effective material properties methyl methacrylate (PMMA) and (10,10) armchair single walled CNTs (SWCNTs), foundation stiffness, shear strains shape functions, semi-vertex angle, γ, a/h and L/a ratios (see, Table 1). The values of the combined load for conical shells reinforced by CNTs are determined for different magnitudes ofλ, within a coupled stress theory context, in order to check for the effect of the FSDST on the critical loading condition. After a systematic numerical computation, it is found that for freely-supported CCSs reinforced by CNTs with linear distributions and resting on the T-P-EF, the critical combined hydrostatic/axial load is reached for $\lambda = 2.4$. The shear strain functions vary parabolically trough the thickness of the cones and given in Table 1, also.

The concept of functionally graded carbon nanotube-reinforced composites (FG-CNTRCs) was defined by Shen [42] to better utilize a low percentage of CNTs in CNTRCs. It is believed that the volume fraction of CNTs varies linearly in the direction of thickness, and such an arrangement of CNTs is easily realized in practice. The distribution of the volume fraction of carbon nanotubes in the thickness direction of the matrix is mathematically expressed by the uniform distribution (UD) and two types of linear function (see, Fig. 2) [11,22]:

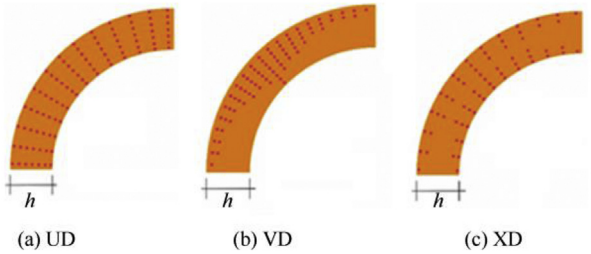

Fig. 2. Different distribution patterns of CNTs in the matrix: (a) UD, (b) VD and (c) XD.

$$\frac{V_{\overline{z}}^{CN}}{V_{*}^{CN}}=\begin{cases}1 & \text{at } UD\\ 1-2\overline{z} & \text{at } VD\\ 4|\overline{z}| & \text{at } XD\end{cases} \tag{16}$$

5.2. Comparison

In this subsection, the values of the separate buckling loads and combined lateral/axial load of unconstrained cylindrical shells reinforced by CNTs with X-type distribution is compared with the results of [11]. The particular case of Eqs. (11), (13) and (15) are used in the comparison. The conical shells revert to the cylindrical shells, if γ tends to zero. The cylinder has radius a and length L_1 with the following geometrical properties: $L_1/h = 30\sqrt{10}$, $L_1/a = \sqrt{10}$, $h = 0.002$ m and $(k_1,k_2) = (0, 0)$, whereas the material properties of CNTs and matrix are assumed as in Table 1 [11]. Based on Table 2, a good agreement between our results and predictions by Shen and Xiang [11] is observable for the separate buckling loads and combined buckling load.

5.3. Specific analysis for CBLs

In what follows, we analyze the sensitivity of the combined buckling loading to heterogeneous profiles, foundation stiffness, volume fractions of CNT, and FSDST formulation, by considering the ratios, $100\%\times\frac{P_{HT}^{wpcb}-P_{HT}^{cb}}{P_{HT}^{cb}}$, $100\%\times\frac{P_{HT}^{cb}-P_{UD}^{cb}}{P_{UD}^{cb}}$ and $100\%\times\frac{P_{1cst}^{cb}-P_{1sdt}^{cb}}{P_{1cst}^{cb}}$. Eqs. (11),

Table 2
Comparative response of buckling loads for shear deformable cylinders reinforced by CNTs with X-type linear distribution.

	T_{sdt}^{axbuc}/MPa	P_{sdt}^{Lbuc}/MPa	P_{sdt}^{cb}/MPa	
			$\mu=140$	$\mu=750$
V_{*}^{CN}	Shen and Xiang [11]			
0.12	118.848	0.285	0.218	0.112
0.17	196.376	0.484	0.37	0.190
0.28	247.781	0.616	0.47	0.242
	Present study			
0.12	117.840	0.281	0.218	0.111
0.17	197.515	0.479	0.371	0.188
0.28	247.062	0.613	0.476	0.2414

Table 3
Variation the CBL for CCSs reinforced by CNTs resting on the T-P-EF within the various shell theories versus the μ for various $V_*^{CN}$and types of CNT distribution.

		$P_{1sdt}^{wpcb} \times 10^6, (n_{cr})$			$P_{1cst}^{wpcb} \times 10^6, (n_{cr})$		
		UD	VD	XD	UD	VD	XD
V_*^{CN}	μ	$(k_1, k_2) = (0, 0)$					
0.12	200	356.163(10)	307.668(9)	420.672(11)	556.866(10)	413.773(8)	775.405(11)
	400	208.748(8)	175.593(7)	251.524(9)	321.301(7)	231.720(6)	461.369(8)
	600	146.280(7)	121.907(6)	177.384(8)	222.898(6)	159.586(5)	322.219(7)
	800	112.156(7)	93.134(6)	136.551(8)	170.290(6)	121.543(5)	246.576(6)
	1000	90.942(7)	75.350(6)	111.000(8)	137.701(5)	98.146(5)	199.492(6)
0.17	200	561.006(9)	478.233(8)	669.354(10)	831.351(9)	614.305(7)	1171.850(10)
	400	325.422(8)	271.034(7)	395.496(9)	475.144(7)	341.942(6)	685.250(8)
	600	227.169(7)	187.420(6)	277.500(8)	328.821(6)	234.986(5)	476.345(6)
	800	174.176(7)	143.185(6)	213.490(7)	251.213(6)	178.968(5)	363.918(6)
	1000	141.230(7)	115.844(6)	173.108(7)	202.911(5)	144.516(5)	294.428(6)
0.28	200	746.947(11)	649.088(9)	855.618(11)	1258.390(11)	930.595(9)	1811.154(12)
	400	443.166(9)	375.549(8)	510.448(9)	741.632(8)	527.047(6)	1085.662(9)
	600	311.451(8)	261.398(7)	360.058(8)	517.077(7)	364.225(6)	759.200(7)
	800	239.758(8)	200.412(6)	277.175(8)	395.330(6)	277.411(5)	581.356(6)
	1000	194.424(7)	162.143(6)	225.311(8)	319.841(6)	224.009(5)	470.345(6)
V_*^{CN}	μ	$(k_1, k_2) = (5 \times 10^8, 3 \times 10^4)$					
0.12	200	445.078(9)	391.908(8)	513.226(10)	644.292(9)	495.282(7)	868.937(11)
	400	255.636(7)	219.381(6)	301.092(8)	365.520(6)	273.152(5)	508.514(7)
	600	177.387(6)	150.968(5)	210.224(7)	251.970(5)	187.295(4)	352.453(6)
	800	135.520(6)	114.979(5)	161.183(7)	191.903(5)	142.275(4)	268.780(5)
	1000	109.642(6)	92.845(5)	130.420(6)	154.962(5)	114.704(4)	217.040(5)
0.17	200	648.009(9)	562.010(8)	759.626(10)	918.239(8)	694.964(7)	1262.122(10)
	400	371.898(7)	314.182(6)	443.916(8)	518.795(6)	382.905(5)	730.649(7)
	600	258.463(6)	216.568(5)	310.023(7)	358.003(5)	263.053(5)	506.046(6)
	800	197.461(6)	164.940(5)	237.701(7)	272.658(5)	199.866(4)	386.027(5)
	1000	159.755(6)	133.189(5)	192.618(6)	220.172(5)	161.135(4)	311.717(5)
0.28	200	838.321(10)	736.091(9)	949.151(11)	1351.298(10)	1014.391(8)	1906.831(11)
	400	492.351(8)	421.095(7)	561.339(9)	788.585(7)	570.025(6)	1133.788(8)
	600	344.310(7)	292.027(6)	393.732(8)	547.162(6)	392.309(5)	790.657(6)
	800	263.990(7)	223.103(6)	302.473(7)	417.995(5)	298.787(5)	604.047(6)
	1000	214.055(7)	180.501(6)	245.259(7)	337.531(5)	241.270(5)	488.300(5)

(13) and (15) are used in numerical calculations.

The variation of CBLs for composite conical shells reinforced by CNTs resting on the T-P-EF within the various shell theory depending on the dimensionless load-proportional parameter, μ, is presented in Table 3 and Fig. 3 for various volume fractions and types of CNT distribution. The following data are used in the creation of tables and graphics: $L/a = 0.5$, $a/h = 25$, $\gamma = 30^\circ$, $(k_1, k_2) = (0, 0)$, $(k_1, k_2) = (5 \times 10^8, 3 \times 10^4)$, $V_*^{CN} = 0.12; 0.17; 0.28$.

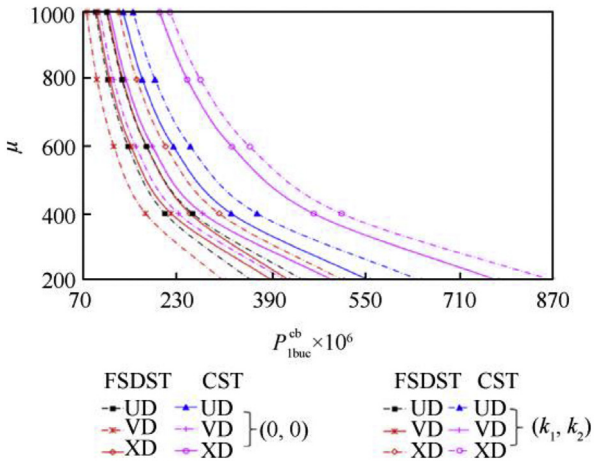

Fig. 3. Variation the values of the CBL for CCSs reinforced by CNTs on the T-P-EF within the various shell theories versus the μ for $V_*^{CN} = 0.12$ and various types of CNT distribution.

Some data is available in the figures or in the table. Although the magnitudes of the CBL increase, its values decrease with increasing of theμ in the presence of T-P-EF. The number of waves corresponding to the CBL reduces with the increase of μ, and this reduce becomes more evident in the presence of the T-P-EF. The composite conical shells reinforced by CNTs with VD and XD-distributions are compared with conical shells reinforced by CNTs with the UD-distribution, the highest and lowest influences of heterogeneity arise for XD-distribution, and vary between (+17.22%) and (+20.57%), and (+13.22%) and (+14.58%) with $V_*^{CN} = 0.17$ and 0.28, respectively, as the μ changes between 200 and 1000.

The influence of VD and XD-distributions on the CBL is weakened, in the presence of T-P-EF. In addition, the use of shear deformation theory significantly reduces the heterogeneity effect on the combined buckling load compared to the classical theory (see, Fig. 3). It is observed that the influence of the T-P-EF on the CBL decreased due to the increase of the μ. It has been determined that the influence of the T-P-EF on the CBL within the framework of FSDST is more pronounced than the classical shell theory. In the presence of the T-P-EF, the influence of shear strains on the CBL decreases with the increase of μ, although it is slow, the highest effect is observed in the CCSs reinforced by CNTs with XD−distribution.

The variation of CBLs of composite conical shells reinforced by the linear distribution of types VD and XD with and without EFs in the context of SDT and CST depending on the ratio $a/h$and compared to the CBL of conical shells reinforced by UD distribution, are plotted in Figs. 4 and 5. The following data are used in the creation of Fig. 4: $L/a = 0.5$, $\gamma = 30^\circ$, $(k_1, k_2) = (0, 0)$, $(k_1, k_2) =$

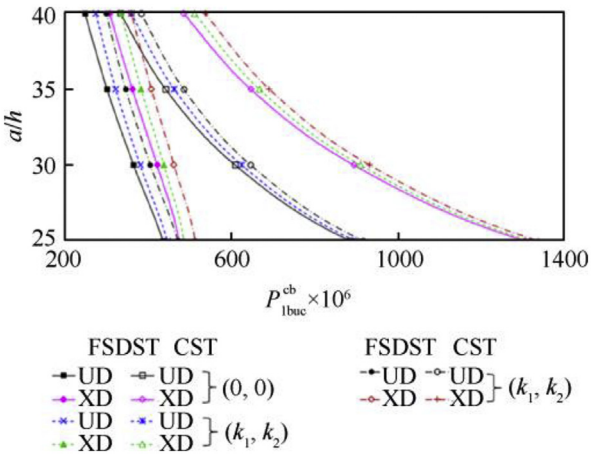

Fig. 4. Variation of CBLs for CCSs reinforced by CNTs with UD- and XD-types distribution with and without EFs versus a/h for $V_*^{CN} = 0.28$.

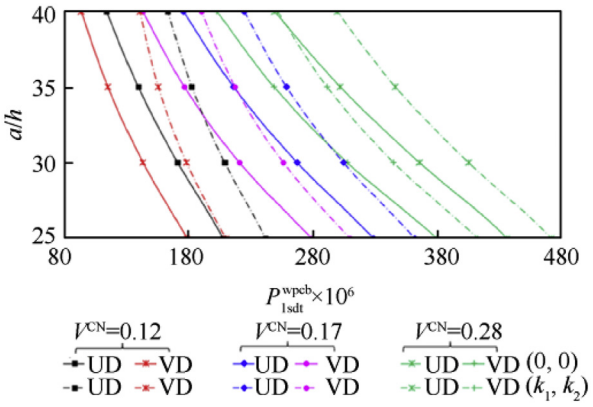

Fig. 5. Variation of P^{wpcb}_{1sdt} and P^{wpcb}_{1cst} for CCSs reinforced by CNTs with UD and VD-types distribution with and without T-P-EF versus R_1/h for a different V_*^{CN}.

$(5 \times 10^8,\ 0)$, $(k_1, k_2) = (5 \times 10^8,\ 3 \times 10^4)$, $V_*^{CN} = 0.28$ and $\mu = 500$. In Fig. 5, $V_*^{CN} = 0.12;\ 0.17;\ 0.28$ and other data are given in Fig. 4. In addition, graphs are drawn in Figs. 4 and 5 using different soil stiffness coefficients. As can be seen from Figs. 4 and 5, the values of CBLs for CCSs reinforced by CNTs with the distribution of UD, VD and XD-shapes, with and without elastic foundations decrease depending on the increase of the ratio a/h, at $V_*^{CN} = 0.12$, 0.17 and 0.28. While the influence of heterogeneity on the CBL for unconstrained CCs based on the FSDST increases from (+8.82%) to (+23.86%), these influences increase from (+8.6%) to (+21.6%) and from (+8.7%) to (+20.6%), in the presence of the one-parameter EF i.e., $(k_1, 0)$ and T-P-EF, respectively, as the ratio a/h increases from 25 to 40. While the influence of shear strains on the CBL of the unconstrained CCS of XD-type, decreases from (+63.61%) to (+36.48%), in the presence of the one- or two-parameter EFs decrease from (+63.1%) to (+34.6%) and from (+50.36%) to (+33%), respectively, as the ratio a/h increases from 25 to 40. As can be seen that the influence of heterogeneity and shear strains on the CBL is less pronounced on the T-P-EF compared to the one-parameter EF or W-EF (see, Fig. 4). The analysis reveals that the influences of one- or two-parameter EFs on the CBLs are more pronounced in the framework of FSDST compared to the classical shell theory. Considering the two-parameter elastic foundation, the influences of heterogeneity on the values of P^{wpcb}_{1sdt} increase from (−14.43%) to (−15.26%) and from (−12.56%) to (−16.04%) for $V_*^{CN} = 0.17$ and 0.28, respectively, as the a/hincreases from 25 to 40. It is observed that the influences of heterogeneity on the P^{wpcb}_{1sdt}reduces by 1–2% in the presence of the T-P-EF compared to unconstrained conical shells (see, Fig. 5).

The variation of the values of the CBL for CCSs reinforced by CNTs (UD, VD and XD) resting on the T-P-EF in the framework of FSDST versus the half-peak angle γ, with the two different volume fractions ($V_*^{CN} = 0.12$ and $V_*^{CN} = 0.17$) are plotted in Fig. 6. The following data are used in the creation of graphics: $L/a = 0.5$, $a/h = 25$, $\gamma = 30^\circ$, $(k_1, k_2) = (2.6\times10^9,\ 3.5\times10^4)$ and $\mu = 500$. As can be seen from Fig. 6, the magnitudes of the CBL decrease with the increasing of half-peak angle γ in the presence of T-P-EF and unconstrained CCSs. This decrease is faster for XD distribution shape at $V_*^{CN} = 0.17$ in the presence of the T-P-EF. When combined buckling loads are examined among themselves for $V_*^{CN} = 0.12$ and $V_*^{CN} = 0.17$, it is observed that the magnitudes of the CBL are higher for XD distribution shape at $V_*^{CN} = 0.17$. In addition, the wave number corresponding to CBLs for CCSs with and without P-E-EF increases due to the increase of the half-peak angle γ in all CNT distribution shapes. It is observed that the influence of the T-P-EF on the values of the CBL in the framework of the FSDST is different in all CNTs reinforcement shapes and volume fractions, and increases with the increase of the half-peak angle γ. It is seen also that the influence of T-P-EF on the combined buckling load is greater than that of others for VD dispersion shape at $V_*^{CN} = 0.12$. For instance, the influence of P-T-EF increases from (+42.67%) to (+54.64%) and from (+27.49%) to (+34.33%) for VD type distribution of CNTs in the matrix at $V_*^{CN} = 0.12$ and $V_*^{CN} = 0.17$, respectively. Additionally, the influence of the T-P-EF on the CBLs increases from (+37.35%) to (+48.94%) and from (+32.29%) to (+44.93%) for UD and XD distribution shapes, respectively at $V_*^{CN} = 0.12$.

The influence of distribution shapes of CNTs on the values of the CBL of CCSs is different and decreases for both with and without ground due to the increase of half-peak angle γ. Furthermore, the influence of the heterogeneity on the CBL of CCSs is smaller in the presence of T-P-EF compared to the groundless case, and the effect of distribution shapes of CNTs at $V_*^{CN} = 0.17$is greater than the case of $V_*^{CN} = 0.12$. For example, for VD type CNT distributions at $V_*^{CN} = 0.17$, the influences of distribution shapes of CNTs on the CBL for CCSs with and without T-P-EF decrease from (−14.71%) to (−12.11%) and from (−11.40%) to (−7.74%), respectively. Besides, the

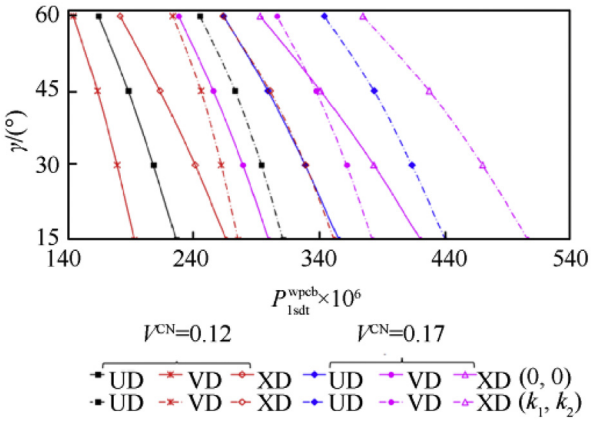

Fig. 6. Variation of CBLs for UD, VD and XD-CCSs with and without T-P-EF within two different shell theories versus the semi-vertex angle, γ, for the different V_*^{CN}.

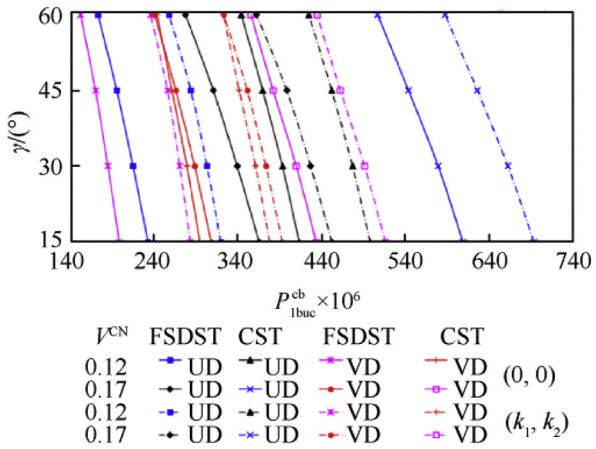

Fig. 7. Variation of CBLs for UD and VD-CCSs with and without T-P-EF in the framework of two different shell theories versus the semi-vertex angle, γ, for the different V_*^{CN}.

effect of distribution shapes of CNTs on the CBL decreases from (+13.19%) to (+7.51%) and from (+14.94%) to (+8.85%), respectively, when the cases $V_*^{CN}=0.12$ and $V_*^{CN}=0.17$ are compared among themselves for the XD distribution shape in the presence of the T-P-EF.

The variation of CBLs of CCSs reinforced by the linear distribution of type VD with and without T-P-EF in the context of two shell theory depending on the semi-vertex angle, γ, and compared to the CBL of composite conical shells reinforced by UD-distribution shape, are illustrated in Fig. 7. The following data are used in the creation of graphics: $L/a=0.5,\ a/h=25,\ \gamma=30^\circ,\ (k_1,\ k_2)=(2.6\times10^9,\ 3.5\times10^4)$and $\mu=500$. It is seen that the values of the CBL decrease depending on the increase of half-peak angle γ with and without T-P-EF. When the combined buckling loads for $V_*^{CN}=0.12$ and $V_*^{CN}=0.17$ are compared with each other, it is observed that the magnitudes of the CBLs of CCSs are smaller for the VD distribution shape of CNTs in the matrix at $V_*^{CN}=0.12$. The influence of soil on the values of CBLs for CNT-based CCSs is more pronounced when using FSDST. Also, the difference between effect of the soil on the CBLs for CNT-based CCSs in the framework FSDST and CST increases with increasing half-peak angle γ. The difference between the combined buckling loads is greater for UD distribution shape at $V_*^{CN}=0.12$. For example, in the presence of the elastic foundation, the difference between the combined buckling loads increases from (+16.85%) to (+25.46%) and (+9.87%) to (+14.53%) for UD distribution shape of CNTs in the matrix at $V_*^{CN}=0.12$ and $V_*^{CN}=0.17$, respectively. Additionally, the difference of the ground effect on the CBLs for UD and VD distribution types of CNTs is (+11.45%) and (+9.49%) at $V_*^{CN}=0.17$and $\gamma=30^\circ$, respectively. It is determined that the influence of shear strains on the values of CBL for CNT-based CCSs with and without T-P-EF increases depending on the increase of half-peak angle γ. Besides, it is revealed that the effect of shear strains on the combined buckling load is greater in the groundless case than the presence of the T-P-EF, and the effect of shear strains is smaller for $V_*^{CN}=0.17$ than for $V_*^{CN}=0.12$. For example, for UD shape of CNTs and at $V_*^{CN}=0.12$, the influence of shear strains on the combined buckling load for CCSs increases from (+43.68%) to (+49.41%) and (+35.80%) to (+38.98%), respectively, in conditions with and without elastic foundations. Moreover, the difference between influences of shear strains on the combined buckling loads without elastic foundation for the VD distribution of CNTs increases from (+3.71%) to (+5.12%) with the increase of half-peak angle γ, as the $V_*^{CN}=0.12$ and $V_*^{CN}=0.17$. Furthermore, the influence of the CNT distribution shapes on the CBL values for CCSs without an elastic foundation within FSDST and CST is more pronounced in the framework of CST at $V_*^{CN}=0.12$. The difference, the effect of CNT distribution shapes on the magnitudes of the CBL within FSDST and CST increases with an increase of the half-peak angle γ, and the largest difference (+17.3%) appears in the CCSs without an elastic foundation for the VD distribution shape at $V_*^{CN}=0.12$ with $\gamma=60^\circ$.

6. Conclusions

In this study the buckling analysis of CCSs reinforced with CNTs subjected to combined loading of hydrostatic pressure and axial compression resting on the T-P-EF. The governing equations of CCSs reinforced by CNTs are derived in the framework of the FSDST that includes shell-foundation interaction. The governing equations are solved by using the Galerkin procedure to determine the combined buckling loads of the structure selected here. The stability equations are solved by using the Galerkin procedure to determine the CBLs of the structure selected here.

Numerical analysis led to the following generalized results:

a) The number of waves corresponding to the values of the CBL reduces with the increase of load-proportional parameter, and this reduce becomes more evident in the presence of the T-P-EF.
b) The influence of VD and XD-distribution shapes on the CBL is weakened, in the presence of T-P-EF, further the use of FSDST significantly reduces the heterogeneity effect on the combined buckling load compared to the CST.
c) Although the magnitudes of the CBL for CNT-based CCSs increase, its values decrease with increasing of the load-proportional parameter in the presence of T-P-EF.
d) In the presence of the T-P-EF, the influence of shear strains on the CBL for CCSs decreases with the increasing of the load-proportional parameter, although it is slow, the highest effect is observed in the CCSs reinforced by CNTs with XD−distribution shape.
e) The influence of heterogeneity and shear strains on the CBL for CCSs reinforced by CNTs is less pronounced on the T-P-EF compared to the one-parameter EF or W-EF.
f) The influences of one- or two-parameter EFs on the CBLs for CCSs reinforced by CNTs are more pronounced in the framework of FSDST compared to the CST.
g) The values of the CBL of composite conical shells reinforced by CNTs with and without T-P-EF decrease for the increasing of the semi-vertex angle.

Declaration of competing interest

The authors declare that they have no known competing financial interests or personal relationships that could have appeared to influence the work reported in this paper.

Appendix A

The differential operators $L_{ij}(i,j=1,2,\ldots,4)$ are defined as

$$L_{11}(\Phi)=\frac{1}{s_2^3e^{3x}}\left(p_{11}\frac{\partial^4}{\partial x^4}+p_{12}\frac{\partial^4}{\partial x^2\partial\bar{\theta}^2}+p_{13}\frac{\partial^3}{\partial x\partial\bar{\theta}^2}+p_{14}\frac{\partial^3}{\partial x^3}+p_{15}\frac{\partial^2}{\partial x^2}+p_{16}\frac{\partial^2}{\partial\bar{\theta}^2}\right)$$

$$L_{12}(w)=\frac{1}{s_2^3e^{3x}}\left(p_{18}\frac{\partial^4}{\partial x^4}+p_{19}\frac{\partial^4}{\partial x^2\partial\bar{\theta}^2}+p_{110}\frac{\partial^3}{\partial x\partial\bar{\theta}^2}+p_{111}\frac{\partial^3}{\partial x^3}+p_{112}\frac{\partial^2}{\partial x^2}+p_{113}\frac{\partial^2}{\partial\bar{\theta}^2}\right)$$

$$L_{13}(\Psi_s)=\frac{1}{s_2^2e^{2x}}\left(p_{115}\frac{\partial^3}{\partial x\partial\bar{\theta}^2}+p_{116}\frac{\partial^3}{\partial x^3}+p_{117}\frac{\partial^2}{\partial x^2}+p_{118}\frac{\partial}{\partial x}+p_{120}\frac{\partial^2}{\partial\delta^2}\right)-J_3\frac{\partial}{\partial x}$$

$$L_{14}(\Psi_\theta)=\frac{1}{s_2^2e^{2x}}\left(p_{121}\frac{\partial^3}{\partial x^2\partial\bar{\theta}}+p_{122}\frac{\partial^2}{\partial x\partial\bar{\theta}}+p_{123}\frac{\partial}{\partial\bar{\theta}}\right)$$

$$L_{21}(\Phi)=\frac{1}{s_2^3e^{3x}}\left(p_{21}\frac{\partial^4}{\partial\delta^4}+p_{22}\frac{\partial^4}{\partial x^2\partial\bar{\theta}^2}+p_{23}\frac{\partial^3}{\partial x\partial\bar{\theta}^2}\right)$$

$$L_{22}(w)=\frac{1}{s_2^3e^{3x}}\left(p_{24}\frac{\partial^4}{\partial x^2\partial\bar{\theta}^2}+p_{25}\frac{\partial^4}{\partial\bar{\theta}^4}+p_{26}\frac{\partial^3}{\partial x\partial\bar{\theta}^2}\right)$$

$$L_{23}(\Psi_s)=\frac{p_{27}}{s_2^3e^{3x}}\frac{\partial^3}{\partial x\partial\bar{\theta}^2}+\frac{p_{28}}{s_2^2e^{2x}}\frac{\partial^2}{\partial\bar{\theta}^2}$$

$$L_{24}(\Psi_\theta)=\frac{1}{s_2^2e^{2x}}\left(p_{29}\frac{\partial^3}{\partial x^2\partial\bar{\theta}}+p_{210}\frac{\partial^2}{\partial x\partial\bar{\theta}}+p_{211}\frac{\partial^3}{\partial\bar{\theta}^3}\right)-J_4\frac{\partial}{\partial\bar{\theta}}$$

$$L_{31}(\Phi)=\frac{1}{s_2e^{x}}\left(p_{31}\frac{\partial^4}{\partial\bar{\theta}^4}+p_{32}\frac{\partial^4}{\partial x^2\partial\bar{\theta}^2}+p_{33}\frac{\partial^3}{\partial x\partial\bar{\theta}^2}+p_{34}\frac{\partial^2}{\partial\bar{\theta}^2}+p_{35}\frac{\partial^4}{\partial x^4}+p_{36}\frac{\partial^3}{\partial x^3}+p_{37}\frac{\partial^2}{\partial x^2}\right)$$

$$L_{32}(w)=\frac{1}{s_2e^{x}}\left(p_{39}\frac{\partial^4}{\partial\bar{\theta}^4}+p_{310}\frac{\partial^4}{\partial x^2\partial\bar{\theta}^2}+p_{311}\frac{\partial^3}{\partial x\partial\bar{\theta}^2}+p_{312}\frac{\partial^2}{\partial\bar{\theta}^2}+p_{313}\frac{\partial^4}{\partial x^4}+p_{314}\frac{\partial^3}{\partial x^3}+p_{315}\frac{\partial^2}{\partial x^2}\right)$$
$$+\cot\gamma\left(\frac{\partial^2}{\partial x^2}-\frac{\partial}{\partial x}\right)$$

$$L_{33}(\Psi_s)=p_{319}\frac{\partial^3}{\partial x\partial\bar{\theta}^2}+p_{320}\frac{\partial^3}{\partial x^3}+p_{321}\frac{\partial^2}{\partial x^2}+p_{322}\frac{\partial}{\partial x}$$

$$L_{34}(\Psi_\theta)=p_{323}\frac{\partial^3}{\partial\bar{\theta}^3}+p_{324}\frac{\partial^3}{\partial x^2\partial\bar{\theta}}+p_{325}\frac{\partial^2}{\partial x\partial\bar{\theta}}+p_{326}\frac{\partial}{\partial\bar{\theta}}$$

$$
\begin{aligned}
&L_{41}(\Phi)=\frac{\cot\gamma}{s_2^3e^{3x}}\left(\frac{\partial^2}{\partial x^2}-\frac{\partial}{\partial x}\right),\\
&L_{42EP}(w)=-\frac{1}{s_2^2e^{2x}}\left(T_{ax}+\frac{1}{2}\frac{xP_H}{\cot\gamma}\right)\left(\frac{\partial^2}{\partial x^2}-\frac{\partial}{\partial x}\right)-\frac{1}{s_2^2e^{2x}}\frac{xP_H}{\cot\gamma}\left(\frac{\partial}{\partial x}+\frac{\partial^2}{\partial\bar{\theta}^2}\right)\\
&L_{42TPEF}(w)=-k_1w+\frac{k_2}{s_2^2e^{2x}}\left(\frac{\partial^2}{\partial x^2}+\frac{\partial^2}{\partial\bar{\theta}^2}\right)=0\\
&L_{43}(\Psi_s)=\frac{J_3}{s_2e^{x}}\frac{\partial}{\partial x}+\frac{J_3}{s_2e^{x}},\ L_{44}(\Psi_\theta)=\frac{\cot\gamma}{s_2e^{x}}\frac{\partial}{\partial\bar{\theta}}
\end{aligned}
\tag{A1}
$$

where p_i are defined as:

$$
\begin{aligned}
&p_{11}=c_{12},\ p_{12}=c_{11}-c_{31},\ p_{13}=4c_{31}-c_{21}-4c_{11},\ p_{14}=c_{11}-5c_{12}-c_{22},\\
&p_{15}=7c_{12}+4c_{22}-4c_{11}-c_{21},\ p_{16}=3c_{21}+3c_{11}-3c_{31},p_{17}=3c_{11}-3c_{12}-3c_{22}+3c_{21},\\
&p_{18}=-c_{13},\ p_{19}=-(c_{14}+c_{32}),\ p_{110}=4c_{14}+4c_{32}+c_{24},\ p_{111}=c_{23}+5c_{13}-c_{14},\\
&p_{112}=4c_{14}-4c_{23}-7c_{13}+c_{24},\ p_{113}=-3(c_{14}+c_{24}+c_{32}),p_{114}=3c_{23}+3c_{13}-3c_{14}-3c_{24},\\
&p_{115}=c_{35},p_{116}=c_{15},p_{117}=-(2c_{15}+c_{25}),p_{118}=2c_{25},p_{119}=-J_3,p_{120}=-c_{35},\ p_{121}=c_{38}+c_{18},\\
&p_{122}=-c_{28}-2c_{18}-2c_{38},\ p_{123}=2c_{28},p_{21}=c_{21},\ p_{22}=c_{22}-c_{31},\ p_{23}=c_{31}-c_{22}+c_{21}.
\end{aligned}
$$

$$
\begin{aligned}
&p_{24}=-c_{32}-c_{23},\ p_{25}=-c_{24},p_{26}=c_{32}+c_{23}-c_{24},p_{27}=c_{25}+c_{35},p_{28}=c_{35},p_{29}=c_{38},\\
&p_{210}=c_{38},p_{211}=c_{28},p_{212}=-J_4,p_{31}=b_{11},p_{32}=b_{31}+b_{21}+b_{12},\ p_{33}=-2b_{31}-3b_{21}-b_{12},\\
&p_{34}=b_{31}+2b_{21}+2b_{11},p_{35}=b_{22},p_{36}=b_{21}-4b_{22}-b_{12},p_{37}=5b_{22}+3b_{12}-3b_{21}-b_{11},\\
&p_{38}=2b_{11}+2b_{21}-2b_{22}-2b_{12},p_{39}=-b_{14},p_{310}=b_{32}-b_{13}-b_{24},p_{311}=b_{13}-2b_{32}+3b_{24},\\
&p_{312}=b_{32}-2b_{24}-2b_{14},p_{313}=-b_{23},p_{314}=b_{13}-b_{24}+4b_{23},p_{315}=b_{14}-3b_{13}+3b_{24}-5b_{23},\\
&p_{318}=2b_{13}-2b_{14}-2b_{24}+2b_{23},p_{319}=b_{35}+b_{15},p_{320}=b_{25},p_{321}=-b_{25}-b_{15},p_{322}=b_{15},\\
&p_{323}=b_{18},p_{324}=b_{38}+b_{28},p_{325}=-b_{28}-b_{18},\ p_{326}=b_{18}.
\end{aligned}
\tag{A2}
$$

in which

$$
\begin{aligned}
&c_{11}=u_{11}^1b_{11}+u_{12}^1b_{21},\ c_{12}=u_{11}^1b_{12}+u_{12}^1b_{21},\ c_{13}=u_{11}^1b_{13}+u_{12}^1b_{23}+u_{11}^2\ ,\ c_{14}=u_{11}^1b_{14}+u_{12}^1b_{24}+u_{12}^2,\\
&c_{15}=u_{11}^1b_{15}+u_{12}^1b_{25}+u_{15}^1,c_{18}=u_{11}^1b_{18}+u_{12}^1b_{28}+u_{18}^1,\ c_{21}=u_{21}^1b_{11}+u_{22}^1b_{21},\ c_{22}=u_{21}^1b_{12}+u_{22}^1b_{22},\\
&c_{23}=u_{21}^1b_{13}+u_{22}^1b_{23}+u_{21}^2,\ c_{24}=u_{21}^1b_{14}+u_{22}^1b_{24}+u_{22}^2,\ c_{25}=u_{21}^1b_{15}+u_{22}^1b_{25}+u_{25}^1,\\
&c_{28}=u_{21}^1b_{18}+u_{22}^1b_{28}+u_{28}^1,\ c_{31}=u_{66}^1b_{31},\ c_{32}=u_{66}^1b_{32}+2u_{66}^2,\ c_{35}=u_{35}^1-u_{66}^1b_{35},\ c_{38}=u_{38}^1-u_{66}^1b_{38}.
\end{aligned}
$$

$$
\begin{aligned}
&b_{11}=\frac{u_{22}^0}{\Delta},\ b_{12}=-\frac{u_{12}^0}{\Delta},\ b_{13}=\frac{u_{12}^0u_{21}^1-u_{11}^1u_{22}^0}{\Delta},\ b_{14}=\frac{u_{12}^0u_{22}^1-u_{12}^1u_{22}^0}{\Delta},b_{15}=\frac{u_{25}^0u_{12}^0-u_{15}^0u_{22}^0}{\Delta},\\
&b_{18}=\frac{u_{28}^0u_{12}^0-u_{18}^0u_{22}^0}{\Delta},b_{21}=-\frac{u_{21}^0}{\Delta},\ b_{22}=\frac{u_{11}^0}{\Delta},\ b_{23}=\frac{u_{11}^1u_{21}^0-u_{21}^1u_{11}^0}{\Delta},\ b_{24}=\frac{u_{12}^1u_{21}^0-u_{22}^1u_{11}^0}{\Delta},\\
&b_{25}=\frac{u_{15}^0u_{21}^0-u_{25}^0u_{11}^0}{\Delta},\ b_{28}=\frac{u_{18}^0u_{21}^0-u_{28}^0u_{11}^0}{\Delta},\ b_{31}=\frac{1}{u_{66}^0},\ b_{32}=-\frac{2u_{66}^1}{u_{66}^0},\ b_{35}=\frac{u_{35}^0}{u_{66}^0},b_{38}=\frac{u_{38}^0}{u_{66}^0},\\
&\Delta=u_{11}^0u_{22}^0-u_{12}^0u_{21}^0.
\end{aligned}
\tag{A3}
$$

where

$$u_{ij}^{t_1}=\int_{-0.5h}^{0.5h}\overline{E}_{ij\bar{\zeta}}z^{t_1}\,\mathrm{d}z,\ (i,j=1,2,6;\ t_1=0,\ 1,\ 2)$$
$$u_{15}^{t_2}=\int_{-0.5h}^{0.5h}z^{t_2}J_{1z}\overline{E}_{11\bar{z}}\mathrm{d}z,\ u_{18}^{t_2}=\int_{-0.5h}^{0.5h}z^{t_2}J_{2z}\overline{E}_{12\bar{z}}\mathrm{d}z,\ u_{25}^{t_2}=\int_{-0.5h}^{0.5h}z^{t_2}J_{1z}\overline{E}_{21\bar{z}}\mathrm{d}z, \tag{A4}$$
$$u_{28}^{t_2}=\int_{-0.5h}^{0.5h}z^{t_2}J_{2z}\overline{E}_{22\bar{z}}\mathrm{d}z,\ u_{35}^{t_2}=\int_{-0.5h}^{0.5h}z^{t_2}J_{1z}\overline{E}_{66\bar{z}}\mathrm{d}z,\ u_{38}^{t_2}=\int_{-0.5h}^{0.5h}z^{t_2}J_{2z}\overline{E}_{66\bar{z}}\mathrm{d}z,\ t_2=0,1.$$

$$J_{iz}=\int_0^z\frac{1}{\overline{E}_{kk\bar{z}}}\frac{\mathrm{d}f_i(z)}{\mathrm{d}z}\mathrm{d}z\ (\ i=1,2;\ k=i+3),$$

$$J_{i+2}=\int_{-0.5h}^{0.5h}\frac{\mathrm{d}f_i}{\mathrm{d}z}\mathrm{d}z(i=1,2)$$

Appendix B

$q_{ij}(i,j=1,2,\ldots,4)$, q_{k_1} and q_{k_2} are parameters and given as

$$q_{14}=\frac{\left[1-e^{s_0(1-2\lambda)}\right]m_2}{s_2^3\left[(2\lambda-1)^2+4m_1^2\right](2\lambda-1)}\Big\{-2p_{121}m_1^2\Big[\times(\lambda-1)\lambda+m_1^2\Big]+p_{122}m_1^2+2p_{123}m_1^2\Big\} \tag{B1}$$
$$q_{21}=\frac{m_2^2m_1^2(1-e^{-2s_0\lambda})}{4\lambda(\lambda^2+m_1^2)s_2^2}\left[p_{21}m_2^2+p_{22}\left(\lambda^2-1+m_1^2\right)-p_{23}\right]$$

$$q_{11}=-\frac{2m_1^2\left[1-e^{s_0(1-2\lambda)}\right]}{\left[(2\lambda-1)^2+m_1^2\right](2\lambda-1)s_2^3}\Big\{p_{11}\Big[3(\lambda-1)(\lambda+1)^3+2m_1^2(\lambda+4)(\lambda+1)-m_1^4\Big]$$
$$-p_{12}m_2^2\left(\lambda^2-\lambda-2+m_1^2\right)\Big\}-\frac{\left[1-e^{s_0(1-2\lambda)}\right]m_1^2}{(2\lambda-1)\left[(2\lambda-1)^2+4m_1^2\right]s_2^3}\Big\{(3p_{13}+2p_{16})m_2^2$$
$$+p_{14}\Big[(\lambda+1)^2(4\lambda-5)+m_1^2(4\lambda+7)\Big]+2p_{15}\Big[\left(\lambda^2-\lambda-2\right)+m_1^2\Big]\Big\}$$

$$q_{12}=-\frac{\left[1-e^{2s_0(1-\lambda)}\right]m_1^2}{4s_2^4\left[(\lambda-1)^2+m_1^2\right](\lambda-1)}\Big\{p_{18}\Big[(3\lambda-4)\lambda^3+2\lambda(\lambda+2)m_1^2-m_1^4\Big]-p_{19}m_2^2\Big[\lambda(\lambda-2)+m_1^2\Big]$$
$$+p_{110}m_2^2+p_{111}\left(2\lambda^3+2\lambda m_1^2-3\lambda^2+m_1^2\right)+p_{112}\Big[\lambda(\lambda-2)+m_1^2\Big]+p_{113}m_2^2\Big\}$$

$$q_{13}=\frac{\left[1-e^{s_0(1-2\lambda)}\right]m_1}{(2\lambda-1)\left[(2\lambda-1)^2+4m_1^2\right]s_2^3}\Big\{p_{115}\Big[(2\lambda-1)\lambda+2m_1^2\Big]m_2^2-p_{116}\Big[(2\lambda-1)\lambda^3+3\lambda m_1^2-2m_1^4\Big]$$
$$-p_{117}\left(m_1^2-\lambda^2+2\lambda^3+2\lambda m_1^2\right)-p_{118}\Big[(2\lambda-1)\lambda+2m_1^2\Big]\Big\}-\frac{\left[1-e^{-s_0(1+2\lambda)}\right]m_1}{(2\lambda+1)\left[(2\lambda+1)^2+4m_1^2\right]s_2^3}$$
$$\times\Big\{-J_3\Big[\lambda(1+2\lambda)+2m_1^2\Big]s_2^2-p_{120}(2\lambda+1)m_2^2\Big\}$$

$$q_{22}=-\frac{\left[1-e^{s_0(1-2\lambda)}\right]m_1^2m_2^2}{\left[(2\lambda-1)^2+4m_1^2\right](2\lambda-1)s_2^3}\left\{2p_{24}\left[\times(\lambda-1)\lambda+m_1^2\right]+2p_{25}m_2^2-p_{26}\right\}$$

$$q_{23}=\frac{m_1m_2^2}{s_2^2}\left\{\frac{p_{27}\left[(2\lambda-1)\lambda+2m_1^2\right]\left[1-e^{s_0(1-2\lambda)}\right]}{\left[(2\lambda-1)^2+4m_1^2\right](2\lambda-1)s_2}+\frac{p_{28}\left(1-e^{-2s_0\lambda}\right)}{4\left(m_1^2+\lambda^2\right)}\right\}$$

$$q_{24}=-\frac{m_1^2m_2}{4}\left\{\frac{\left[p_{29}\left(m_1^2+\lambda^2\right)+p_{211}m_2^2\right]\left(1-e^{-2\lambda s_0}\right)}{s_2^2\left(m_1^2+\lambda^2\right)\lambda}+\frac{J_4\left(1-e^{-2(\lambda+1)s_0}\right)}{(\lambda+1)\left[(\lambda+1)^2+m_1^2\right]}\right\} \tag{B2}$$

$$\begin{aligned}q_{31}=&\frac{1}{4}\frac{m_1^2\left(1-e^{-2\lambda s_0}\right)}{\lambda\left(m_1^2+\lambda^2\right)s_2^3}\left\{p_{31}m_2^4+p_{32}m_2^2\left(\lambda^2+m_1^2-1\right)-p_{33}m_2^2-p_{34}m_2^2\right.\\&+p_{35}\left[m_1^4-(\lambda+1)^3(3\lambda-1)-2(\lambda+3)(\lambda+1)m_1^2\right]-p_{36}\left(2m_1^2\lambda+3\lambda^2+2\lambda^3+3m_1^2-1\right)\\&\left.-p_{37}\left(m_1^2+\lambda^2-1\right)\right\}\end{aligned}$$

$$\begin{aligned}q_{32}=&-\frac{\left[1-e^{s_0(1-2\lambda)}\right]m_1^2}{(2\lambda-1)\left[(2\lambda-1)^2+4m_1^2\right]s_2^4}\left\{2p_{39}m_2^4+2p_{310}\left(\lambda^2-\lambda+m_1^2\right)\right.\\&-p_{311}m_2^2-2p_{312}m_2^2+2p_{313}\left[(2-3\lambda)\lambda^3-2m_1^2\lambda(\lambda+1)+m_1^4\right]\\&\left.-p_{314}\left(4\lambda^3-3\lambda^2+4m_1^2\lambda+m_1^2\right)-2p_{315}\left(\lambda^2-\lambda+m_1^2\right)\right\}+\frac{\cot\gamma\left(1-e^{-2s_0\lambda}\right)m_1^2}{4\lambda s_2^3}\end{aligned}$$

$$q_{33}=\frac{m_1\left(1-e^{-2\lambda s_0}\right)}{4s_2^3\lambda}\left[p_{319}m_2^2-p_{320}\left(\lambda^2-m_1^2\right)-p_{321}\lambda-p_{322}\right]$$

$$q_{34}=\frac{\left(1-e^{-2\lambda s_0}\right)m_1^2m_2}{4\lambda\left(m_1^2+\lambda^2\right)s_2^3}\left[p_{326}-p_{323}m_2^2-p_{324}\left(m_1^2+\lambda^2\right)\right] \tag{B3}$$

$$q_{41} = -\frac{\left(1-e^{-2s_0\lambda}\right)m_1^2\cot\gamma}{4\lambda s_2^2},\ q_{42EP} = -Pq_{P_H} - T_{ax}q_T;\ q_{42TPEF} = -k_1q_{k_1} - k_2q_{k_2}$$

$$q_{43} = -\frac{m_1J_3}{s_2}\frac{\left[1-e^{-s_0(2\lambda+1)}\right]\left[\left(2\lambda^2+2m_1^2+3\lambda+1\right)\right]}{\left[(2\lambda+1)^2+4m_1^2\right](2\lambda+1)} \tag{B4}$$

$$q_{44} = \frac{2J_4m_1^2m_2}{s_2}\frac{\left[1-e^{-s_0(2\lambda+1)}\right]}{\left[(2\lambda+1)^2+4m_1^2\right](2\lambda+1)}$$

where

$$q_{P_H} = -\frac{\left[2m_1^2+2\lambda^2+2\lambda+1+4m_2^2\right]m_1^2}{2s_2\cot\gamma}\frac{\left[1-e^{-s_0(2\lambda+1)}\right]}{\left[(2\lambda+1)^2+4m_1^2\right](2\lambda+1)},$$

$$q_T = -\frac{1}{4}\frac{m_1^2\left(1-e^{-2s_0\lambda}\right)}{s_2^2\lambda}, \tag{B5}$$

$$q_{k_1} = -\frac{m_1^2\left[1-e^{-2(\lambda+1)s_0}\right]k_1}{4\left[(\lambda+1)^2+4m_1^2\right]\left(\lambda+1\right)}\ q_{k_2} = -\frac{m_1^2\left(\lambda^2+m_1^2+m_2^2\right)}{4s_2^2}\frac{\left(1-e^{-2\lambda s_0}\right)}{(\lambda^2+m_1^2)\lambda}$$

References

[1] Du JH, Bai J, Cheng HM. The present status and key problems of carbon nanotube-based polymer composites. Express Polym Lett 2007;1:253–73.
[2] Cai D, Song M. Latex technology as a simple route to improve the thermal conductivity of a carbon nanotube/polymer composite. Carbon 2008;46:2107–12.
[3] Iijima S, Ichihashi T. Single-shell carbon nanotubes of 1-nm diameter. Nature 1993;363:603–5.
[4] Dai H. Carbon nanotubes: synthesis, integration and properties acc. Chem Res 2003;35:1035–44.
[5] Moisala A, Li Q, Kinloch IA, Windle AH. Thermal and electrical conductivity of single- and multi-walled carbon nanotube-epoxy composites. Compos Sci Technol 2006;66:1285–8.
[6] Xie XL, Mai YW, Zhou XP. Dispersion and alignment of carbon nanotubes in polymer matrix: a review. Mater Sci Eng R 2005;49(4):89–112.
[7] Velasco-Santos C, Martínez-Hernández AL, Fisher FT, Ruoff R, Castaño VM. Improvement of thermal and mechanical properties of carbon nanotube composites through chemical functionalization. Chem Mater 2003;15:4470–5.
[8] Moniruzzaman M, Winey KI. Polymer nanocomposites containing carbon nanotubes. Macromolecules 2006;39:5194–205.
[9] Alizada AN, Sofiyev AH. Modified Young's moduli of nano-materials taking into account the scale effects and vacancies. Meccanica 2011;46:915–20.
[10] Díez-Pascual AM, Guan J, Simard B, Gómez-Fatou MA. Poly (phenylene sulphide) and poly (ether ether ketone) composites reinforced with single-walled carbon nanotube buckypaper: I – structure, thermal stability and crystallization behaviour. Compos Appl Sci Manuf 2012;43(6):997–1006.
[11] Shen HS, Xiang Y. Postbuckling of nanotube-reinforced composite cylindrical shells under combined axial and radial mechanical loads in thermal environment. Compos B Eng 2013;52:311–22.
[12] Sahmani S, Aghdam MM, Bahrami M. Nonlinear buckling and postbuckling behavior of cylindrical nano-shells subjected to combined axial and radial compressions incorporating surface stress effects. Compos B Eng 2015;79:676–91.
[13] Heydarpour Y, Malakzadeh P. Dynamic stability of rotating FG-CNTRC cylindrical shells under combined static and periodic axial loads. Int J Struct Stabil Dynam 2018;18. https://doi.org/10.1142/S0219455418501511.
[14] Sofiyev AH, Tornabene F, Dimitri R, Kuruoglu N. Buckling behavior of FG-CNT reinforced composite conical shells subjected to a combined loading. Nanomaterials 2020;10(3):1–19.
[15] Pasternak PL. On a new method of analysis of an elastic foundation by means of two foundation constantsvol. 1. Moscow: State Pub House Lit Construct Archite; 1954. 1–56 [in Russian].
[16] Kerr AD. Elastic and viscoelastic foundation models. ASME J App Mech 1964;31:491–8.
[17] Vlasov VZ, Leontiev NN. Beams, plates and shells on an elastic foundation. Moscow: Fizmatgiz; 1960.
[18] Sun B, Huang Y. The exact solution for the general bending problems of conical shells on the elastic foundation. Appl Math Mech 1988;9:455–69.
[19] Zhang LW, Lei Z, Liew KM. Computation of vibration solution for functionally graded carbon nanotube-reinforced composite thick plates resting on elastic foundations using the element-free IMLS-Ritz method. Appl Math Comput 2015;256:488–504.
[20] Fu Y, Zhong J, Shao X, Tao C. Analysis of nonlinear dynamic stability for carbon nanotube-reinforced composite plates resting on elastic foundations. Mech Adv Mater Struct 2016;23(11):1284–9.
[21] Baníc D, Bacciocchi M, Tornabene F, Ferreira A. Influence of Winkler-Pasternak foundation on the vibrational behavior of plates and shells reinforced by agglomerated carbon nanotubes. Appl Sci 2017;7:1228.
[22] Soltani K, Bessaim A, Houari MSA, Kaci A, Benguediab M, Tounsi A, MSh Alhodaly. A novel hyperbolic shear deformation theory for the mechanical buckling analysis of advanced composite plates resting on elastic foundations. Steel Compos Struct 2019;30(1):13–29.
[23] Bendenia N, Zidour M, Bousahla AA, Bourada F, Tounsi A, Benrahou KH, Bedia EAA, Mahmoud SR. Deflections, stresses and free vibration studies of FG-CNT reinforced sandwich plates resting on Pasternak elastic foundation. Comput Concr 2020;26(3):213–26.
[24] Rabhi M, Benrahou KH, Kaci A, Houari MSA, Bourada F, Bousahla AA, Tounsi A, Bedia EAA, Mahmoud SR, Tounsi A. A new innovative 3-unknowns HSDT for buckling and free vibration of exponentially graded sandwich plates resting on elastic foundations under various boundary conditions. Geomech Eng 2020;22(2):119–32.
[25] Refrafi S, Bousahla AA, Bouhadra A, Menasria A, Bourada F, Tounsi A, Bedia AAA, Mahmoud SR, Benrahou KH, Tounsi A. Effects of hygro-thermo-mechanical conditions on the buckling of FG sandwich plates resting on

elastic foundations. Comput Concr 2020;25(4):311–25.
[26] Shen HS, Xiang Y. Postbuckling of axially compressed nanotube-reinforced composite cylindrical panels resting on elastic foundations in thermal environments. Compos B Eng 2014;67:50–61.
[27] Shen HS, Xiang Y. Nonlinear response of nanotube-reinforced composite cylindrical panels subjected to combined loadings and resting on elastic foundations. Compos Struct 2015;131:939–95.
[28] Shen HS, Xiang Y. Postbuckling of pressure-loaded nanotube-reinforced composite doubly curved panels resting on elastic foundations in thermal environments. Int J Mech Sci 2016;107:225–34.
[29] Shen HS, Xiang Y. Thermal postbuckling of nanotube-reinforced composite cylindrical panels resting on elastic foundations. Compos Struct 2015;123:383–92.
[30] Mohammadi M, Arefi M, Dimitri R, Tornabene F. Higher-order thermo-elastic analysis of FG-CNTRC cylindrical vessels surrounded by a Pasternak foundation. Nanomaterials 2019;9(1). Article Number: 79.
[31] Duc ND, Cong PH, Tuan ND, Tran P, Thanh NV. Thermal and mechanical stability of functionally graded carbon nanotubes (FG CNT)-reinforced composite truncated conical shells surrounded by the elastic foundations. Thin-Walled Struct 2017;115:300–10.
[32] Ambartsumian SA. Theory of anisotropic shells. Moscow: State Pub House Phys Math Lit; 1961.
[33] Reddy JN, Liu CF. A higher-order shear deformation theory of laminated elastic shells. Int J Eng Sci 1985;23:319–30.
[34] Aydogdu M. A new shear deformation theory for laminated composite plates. Compos Struct 2009;89:94–101.
[35] Carrera E. The effects of shear deformation and curvature on buckling and vibrations of cross-ply laminated composite shells. J Sound Vib 1991;150(3):405–33.
[36] Bousahla AA, Bourada F, Mahmoud SR, Tounsi A, Algarni A, Bedia EAA, Tounsi A. Buckling and dynamic behavior of the simply supported CNT-RC beams using an integral-first shear deformation theory. Comput Concr 2020;25(2):155–66.
[37] Babaei H, Kiani Y, Eslami M. Thermal buckling and post-buckling analysis of geometrically imperfect FGM clamped tubes on nonlinear elastic foundation. Appl Math Model 2019;71:12–30.
[38] Sobhy M, Zenkour AM. Vibration analysis of functionally graded graphene platelet-reinforced composite doubly-curved shallow shells on elastic foundations. Steel Compos Struct 2019;133(2):195–208.
[39] Sobhy M, Zenkour AM. A comprehensive study on the size-dependent hygrothermal analysis of exponentially graded microplates on elastic foundations. Mech Adv Mater Struct 2020;27(10):816–30.
[40] Volmir AS. Stability of elastic systems. Nauka: moscow. English translation: foreign tech. Division, air force systems command. Ohio: Wright-Patterson Air Force Base; 1967.
[41] Eslami MR. Buckling and postbuckling of beams, plates and shells. Ist Springer; 2018.
[42] Shen HS. Nonlinear bending of functionally graded carbon nanotube-reinforced composite plates in thermal environments. Compos Struct 2009;91:9–19.